Comparison of Piezoelectric, Magnetostrictive, and Electrostrictive Hybrid Hydraulic Actuators

SHAJU JOHN,[1] JAYANT SIROHI,[1] GANG WANG[2] AND NORMAN M. WERELEY[1,*]

[1]*Smart Structures Laboratory, Department of Aerospace Engineering*
University of Maryland, College Park, MD 20742, USA

[2]*Techno-Sciences Inc., 11750 Beltsville Drive*
3rd floor, Beltsville, MD 20705, USA

ABSTRACT: In recent years, active material driven actuators have been widely researched for potential applications in the fields of aerospace, automotive, and civil engineering. While most of these active materials, such as piezoelectric, magnetostrictive, and electrostrictive materials, have high force and bandwidth capabilities, they are limited in stroke. In combination with hydraulic systems, the field-dependent motion of these materials can be amplified to produce high force, high stroke actuators. In a hybrid hydraulic pump, the motion of an active material is used to pressurize a hydraulic fluid. Since the properties of active materials vary greatly in terms of free strain and block force, there is a need to identify the optimum active material for a particular application. This study compares four active materials, Lead–Zirconate–Titanate (PZT), Lead–Magnesium–Niobate (PMN), Terfenol-D and Galfenol, as the drivers of a hybrid hydraulic actuation system. The performance of each of these active materials has been evaluated in the same hydraulic actuator through systematic testing of the actuator while maintaining the same length and volume for each active material. In each case, the active material has a length of around 54 mm and a cross-sectional area of 25 mm^2. Commonly used metrics such as output power and electromechanical efficiency are used for comparison. Of the four materials tested in this study, PMN presented the largest free strain (2000 με), while Galfenol presented the least (300 με). The highest no-load velocity is also exhibited by the PMN-based actuator (270 mm/s). The maximum output power obtained is 2.5 W for both PMN and Terfenol-D-based actuators while the highest electromechanical efficiency obtained is 7% for the PMN-based actuator.

Key Words: piezoelectric, magnetostrictive, electrostrictive, hybrid actuator, power, efficiency.

INTRODUCTION

ACTIVE materials are materials that undergo an induced strain due to the application of an electric, magnetic or thermal field. Within this broad classification of active materials, we investigate the properties of electro-active and magneto-active materials, which respond to electric and magnetic fields, respectively. In recent years, hybrid actuators have exploited the high energy density, large blocked force, and large actuation bandwidth capability of active materials by using them as primary driving elements in actuators. Additionally, hybrid actuators can be designed to have a very low number of moving parts, thus improving their reliability. Actuation systems based on active materials find applications in rotorcraft (Prechtl and Hall, 1999), automobile (Lam and Liao, 2003), and biomedical (Shoji and Esashi, 1994) engineering. Despite their high energy density and actuation bandwidth, the factor that limits the use of such actuators is their low induced strain. Frequency rectification methods overcome the low induced strain by trading high frequency motion of the active material for a low frequency motion of the load through the use of active or passive means. Examples of such frequency rectified devices are ultrasonic motors (Sashida and Kenjo, 1993; Uchino, 1997), rotary piezoelectric motors (Duong and Garcia, 1996; Frank et al., 2003), and inch-worm motors (Hemsel and Wallaschek, 2000; Galante et al., 2000). Because such devices use friction for rectification, they are highly prone to rapid wear and tear. Hybrid hydraulic devices are another class of devices that use frequency rectification techniques to convert low amplitude, high frequency motion of the active material

*Author to whom correspondence should be addressed.
E-mail: wereley@umd.edu
Figures 1, 2, 5–7 and 9–11 appear in color online: http://jim.sagepub.com

1045-389X/07/10 1035–14 $10.00/0 DOI: 10.1177/1045389X06072355
© SAGE Publications 2007
Los Angeles, London, New Delhi and Singapore
Downloaded from http://jim.sagepub.com by UNIVERSITY OF MARYLAND on May 3, 2009

into a high amplitude, low frequency motion of the load. In these actuators, the active material is used to pressurize a hydraulic fluid in an enclosed pumping chamber. The bidirectional motion of this pressurized fluid, resulting from the excitation of the active material, is then rectified using one-way valves. These one-way valves, which act in a similar manner to electric diodes, allow flow in only one direction depending on the pressure difference across them. This results in a unidirectional flow exiting the pump and thus, a unidirectional motion of the output load. To obtain bidirectional motion of the output load, an additional valving system (active or passive) must be introduced. Several such hybrid hydraulic devices have been developed in recent years by various research groups (Mauck and Lynch, 2000; Nasser et al., 2000; Sirohi and Chopra, 2003). These different prototypes of the hybrid hydraulic actuator vary in the output power capability and frequency range of operation.

A variety of models have been developed to predict the performance of hydraulic hybrid actuators, such as quasi-static approaches (Mauck et al., 2001; Cadou and Zhang, 2003), lumped parameter approaches using electrical analogies (Nasser and Leo, 2000), and mechanical analogies (Oates and Lynch, 2001), transmission line (Sirohi et al., 2005) approaches, CFD methods (John et al. (2006); Oates and Lynch, 2001) and integration of the mass conservation equations (Konishi et al., 1997; Konishi et al., 1998; Regelbrugge et al., 2003). Such models attempt to address the overall performance of the actuators vis-a-vis fluid losses, hydraulic resonances, output power, and electromechanical efficiency. The performance of hybrid hydraulic actuation systems depends on several factors like pump head design, hydraulic circuit dynamics, and electric drive circuit design. The properties of the active driving material are also highly critical to the performance of a hybrid hydraulic actuator. Therefore, investigation into the impact of different active material stacks on the performance of hybrid hydraulic actuator systems becomes important. There have been several studies that compared the bulk material properties – mechanical and electrical – of different active materials (Pan et al., 2000; Zhao and Zhang, 1996; Pomirleanu and Giurgiutiu, 2004). Studies into a comprehensive comparison of these active materials from an application point of view have been few (Janocha et al., 1994; Ellison, 2004; Damjanovic and Newnham, 1992).

A frequency-rectified device makes use of the high bandwidth capability of the active material by driving the active material stack at high frequencies. This ensures that the maximum volume of fluid is displaced at a very high frequency to result in maximum obtainable volume flow rate from the pumping chamber. The limitations of operating at higher pumping frequencies are the increase in input power required and the reduction in flow rate after resonance of the hydraulic circuit is reached. The resonance of the hydraulic circuit depends on the inertia and stiffnesses of the fluid lines, the active material stack, and the load. The maximum flow rate is obtained at the resonant frequency of the actuator system. Raising the pumping frequency beyond this value results in a decrease in the performance of the actuator. The amount of energy transferred from the active material to the fluid is governed primarily by the impedance matching condition between the active material stack and the fluid in the pumping chamber. Thus, to transfer the maximum energy from the active material to the fluid, the active material stack stiffness should match the fluid chamber stiffness (Sirohi, 2002). The overall electromechanical efficiency of the actuator determines the total amount of energy transferred to the load as a fraction of the amount of energy put into the material. In this study, energy is measured in terms of the rate of work done, i.e., power. The stiffness of the active material stack also affects the overall electromechanical efficiency since the energy output of the device is affected by the material stiffness. The input energy depends on the inherent characteristics of the active material and the electric or magnetic drive circuit. The amount of energy consumed by electroactive materials such as piezoelectrics and electrostrictives, depends on the capacitance of the stack. The amount of energy consumed by a magneto-active material depends on the resistance and inductance of the field generating coil. Thus, the design of the magnetic circuit becomes an important consideration for magneto-active materials. Preliminary investigation into the issues of coil design was done in a previous work (Ellison, 2004) and will not be addressed in this article.

This study compares different active materials from an actuator system performance standpoint while constraining the volume of the active material and the volume of the actuator as a whole. Most applications place geometric and volumetric constraints on the actuator. Thus it is necessary to evaluate the performance of the active material stacks as drivers for hybrid actuators on the basis of their active length, cross-sectional area, active volume, and overall actuator dimensions. The active material stacks used in the study had a length of around 54 mm and a cross-sectional area of 25 mm^2. The actuation system used in this study was developed at the Alfred Gessow Rotorcraft Center (Sirohi and Chopra, 2003). By adapting the different materials to be used in the same actuator, the overall dimensions of the actuator were also held constant. This provides the basis for a direct comparison between these materials.

Downloaded from http://jim.sagepub.com at UNIV OF MARYLAND on August 3, 2009

MATERIAL PROPERTIES

Active materials vary widely in their basic mechanism of strain generation as well as their stiffness, strain, hysteresis, and electrical impedance properties. The stiffness and the amount of strain generated by the material are the major factors that determine its energy output of the actuator. The stiffness of the stack – dictated by Young's modulus of elasticity of the pure active material and the insulating material as well as the cross-sectional area and length of the stack – determines the amount of energy transferred by the stack to the fluid in the pumping chamber through an impedance matching criteria. The free displacement determines the amount of volumetric displacement produced by the stack under no-load conditions. The input electrical energy required by the stack depends on the electrical impedance of the stack or the coil and the hysteresis in the active material. Hysteresis constitutes the part of the input energy that is dissipated within the material and is a characteristic of the bulk material. The rest of the energy is available to be transmitted to the load as useful mechanical work. In the case of electro-active stacks, this part of the input energy (non-dissipative part) is determined by the electrical impedance of the stack, which is capacitive in nature. For magnetostrictive stacks, the non-dissipative part of the input energy depends on the inductance of the magnetic field generating coil. Both electro-active and magneto-active materials shall be referred to as *stacks* in this study.

Electro-active materials produce induced strain on the application of an electric field. The two types of electro-active materials considered for this study are piezoelectric and electrostrictive materials.

- Piezoelectric materials generate strain when an electric field is applied in a prescribed direction. This effect is also called the *converse* effect. The most common form of piezoceramics is based on Lead–Zirconate–Titanate (PZT) compounds. In piezoceramics, the unit cell has a certain degree of asymmetry which gives it a permanent dipole. A poling operation is done on a bulk material to orient all the dipoles in a preferred direction to produce a net polarization. Once polarized, an applied electric field in the poling direction produces a temporary expansion in the poling direction, thus producing induced strain. The piezoelectric stack used in this study was a commercially available stack PST 150/(5×5×54) obtained from American Piezo International Ltd. The free strain and modulus of elasticity of the stack as provided by the manufacturer are 1600 μs and 70 GPa. The stack has a length of 54 mm, a cross-sectional area of 25 mm^2 and is rated for voltages ranging from −20 to 150 V. Figure 1(a) presents the results of static tests done on the PZT stack and shows that the strain is nearly proportional to the voltage applied to the stack. As mentioned earlier, the energy consumption of a stack depends on its electrical impedance. The electrical impedance of piezoelectric stacks is capacitive in nature and has a value of 5.4 μF. Due to its capacitive nature, the impedance decreases with increase in frequency and the current required to maintain a constant voltage increases.
- Electrostrictive materials also exhibit strain on the application of electric field. The phenomenon of electrostriction, however, is fundamentally different from the converse piezoelectric effect. The unit cell in an electrostrictive material is centro-symmetric and hence, the strain exhibited by such a material is not due to the change in structure, but is inherent in the material itself. The basic mechanism of actuation is a separation of charged ions in the unit cell of the material. The electrostrictive stack used in this study was a commercially obtained stack TRS PMN-5% PT, a Lead–Magnesium–Niobate (PMN) compound, from TRS Ceramics Inc. The free strain and modulus of elasticity of this stack as provided by the manufacturer are 2000 μs and 20 GPa, respectively.

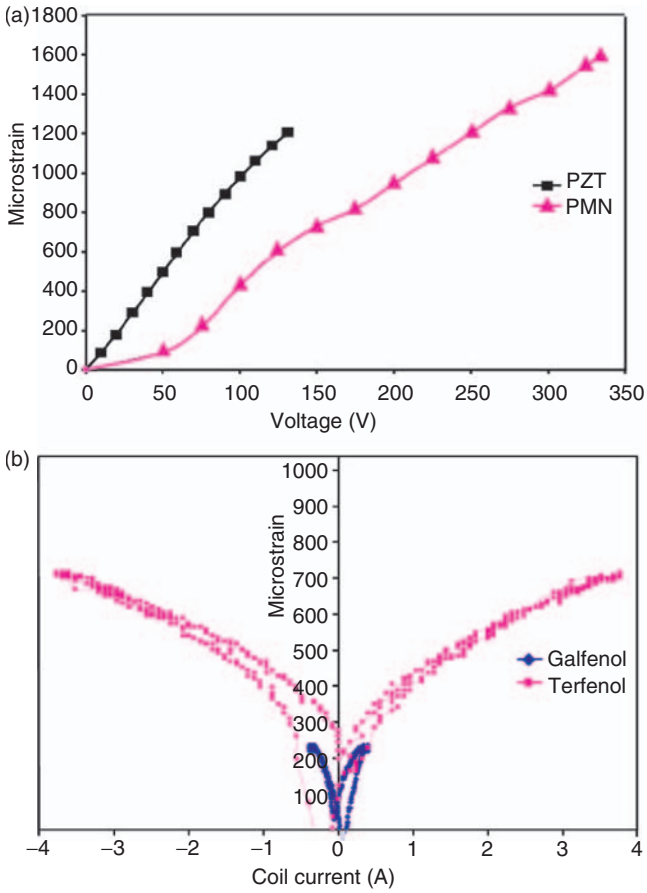

Figure 1. *The static relationship between strain in the material and applied excitation field; (a) electro-active stacks and (b) magneto-active stacks.*

Downloaded from http://jim.sagepub.com at UNIV OF MARYLAND on August 3, 2009

The stack has an overall length of 59 mm and a cross-sectional area of 24 mm^2. The relationship between strain and applied voltage for this stack is shown in Figure 1(a). Electrostriction is fundamentally similar to magnetostriction and exhibits many common characteristics. Typically, the strain exhibited by an electrostrictive material has a quadratic relationship with the applied field and shows the property of *frequency doubling*. This phenomenon will be further explained in relation to the magnetostrictive stack. Ideally, an electrostrictive stack can operate under both positive and negative electric fields. However, due to the recommendations of the manufacturer, the electrostrictive stack used in this study was rated only for the voltage range of −20 to 500 V. The electrical impedance of an electrostrictive stack, like a piezoelectric stack, is capacitive in nature and has a value of 0.37 μF. Because the PMN stack has a lower capacitance than the PZT stacks, its energy consumption at a given voltage and frequency is lower.

Application of preload does not have a marked effect on the strain output of piezoelectric materials. Preload is generally applied to these stacks to ensure that the stack always remains in contact with the actuator piston during high frequency operation. Application of preload also offsets the effect of tensile stress in the stack. Extensional strains are highly detrimental to the integrity of the stacks. Special care is required while mounting the stack in the actuator body as the slightest misalignment can produce a bending moment on the stack. Especially in stacks with a large aspect ratio (ratio of length to cross-sectional width), this bending moment can result in extensional stresses during high frequency operation. To mitigate the effect of extensional strains produced by bending moments, ball ends are used as the contact points on either end of the stack.

The type of magneto-active material considered in this study are magnetostrictive alloys. Magnetostrictive materials require an externally applied magnetic field to exhibit strain. This effect, called *Joule* effect, is generated from the realignment of magnetic domains in the material. Without an external field, the magnetic domains in a magnetostrictive material stacks will be aligned randomly. When an external magnetic field is applied, the domains realign in the preferred orientation parallel to the external magnetic induction B of the coil. This realignment causes a change in dimension. The response bandwidth of magnetostrictive materials are typically large (~1 kHz). In contrast to piezoelectrics, preloading a magnetostrictive material has a significant effect on the induced strain obtained from the sample. The strain obtained from a magnetostrictive material increases substantially with an increase in preload. The magnetic domains tend to align under the effect of the preload and strain can be obtained from the stack by applying a magnetic field large enough to offset this initial domain alignment. This effect is a marked difference when compared to electro-active materials, where there is no significant effect of preload on the strain obtained. A typical static behavior of a magnetostrictive material is shown in Figure 1(b). In addition to the longitudinal extension, the magnetostrictive material also undergoes a lateral contraction. The net result is a zero change in net volume of the material. Another distinctive feature of magnetostrictive materials is that the displacement of the material in its normal direction is always positive, regardless of the applied magnetic field direction. This can also be seen in Figure 1(b). Thus, the strain has a quadratic dependence on the applied field. This means that when a purely AC sinusoidal signal is applied to the sample, the output strain will have a frequency which is double that of the input signal. This property of magnetostrictive material can be used to perform a *frequency doubling* of the stack. Because of this phenomenon, a bidirectional motion of the stack can be obtained only by operating about a bias point. At the bias point, the magnetic domains are preferentially oriented. Thus, the length of the sample can be increased or decreased by increasing or decreasing the applied magnetic field about this bias point. Two types of magnetostrictive material were used in this study.

- Terfenol-D is an inter-metallic alloy of Terbium, Dysprosium, and Iron that is produced as a near-single crystal. Terfenol-D is highly brittle and is likely to crack after prolonged operation. It has a maximum free strain and Young's modulus values of 1000 μs and 35–50 GPa, respectively. This material was a commercially available product provided by Etrema Products Inc.
- Galfenol, an alloy of Gallium and Iron, and unlike Terfenol-D, has a much better ductility and so has a high degree of structural integrity. Galfenol has been shown to be machinable and has a maximum free strain and Young's modulus of 300 μs and 20–25 GPa, respectively. This research material was manufactured by Tom Lograsso of Iowa State University.

Both stacks have a length of 54.8 mm and a cross-sectional area of 31 mm^2. As opposed to electro-active stacks, the maximum free strain obtainable from a magnetostrictive stack is a strong function of the applied preload. The required magnetic field is applied using a field generating coil wound using 24 gage copper wire. It is also necessary to have flux return paths for the magnetic field lines. The main body of the pump is made of steel and thus acts as the flux return. The energy consumption of a magnetostrictive material depends on the electrical impedance of the coil, which is predominantly inductive in nature. An important fact

Downloaded from http://jim.sagepub.com at UNIV OF MARYLAND on August 3, 2009

Table 1. Manufacturer supplied material properties.

Parameter	PZT	PMN	Terfenol-D	Galfenol
Length (mm)	54	59	54.8	54.8
Cross-sectional area (mm^2)	25	24	31	31
Free strain (μs)	1600	2000	1000	300
Field required for max. strain	120 V	500 V	80 kA/m	25 kA/m
Young's modulus (GPa)	70	20	35–50	20–25
Stiffness of stack (MN/m)	20	8.1	28.3	14.2
Blocked force (N)	1700	900	1550	310
Capacitance (μF)	5.4	0.37	–	–
Magnetic permeability	–	–	3–10	300
Robustness	Robust	Brittle	Brittle	Machinable

to remember about the magnetic circuit is that for a given current, the magnetic field experienced by each stack depends on its magnetic permeability. Thus, equivalence in applied current does not translate to an equivalence in magnetic field as experienced by the different magnetostrictive stacks.

Table 1 shows the salient material properties of the four samples. The overall geometrical properties of the actuator were held constant in all four cases. Figure 2 shows the active material stacks used in this study.

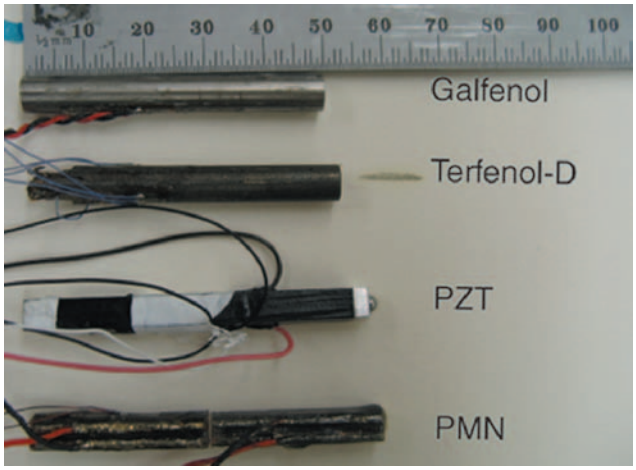

Figure 2. *The four active material stacks used in this study.*

EXPERIMENTAL SETUP

A schematic diagram of the hybrid actuator used in this study is given in Figure 3. The basic operation of the actuation system is executed in three stages. In the first stage, a driving signal is generated using a signal generator and is amplified and applied across the PMN/PZT stack or the coil surrounding the Terfenol-D/Galfenol stack. The changing electric/magnetic field applied to the active material produces induced strain in the material and pushes a piston which causes the fluid in the pumping chamber to be pressurized. In the next step, two oppositely oriented unidirectional check valves respond to the fluid pressure by opening only in their preferred direction. Thus, the check valves perform the function of rectification and convert the oscillatory motion of the active material stack to a unidirectional motion of the fluid. In the third stage, the fluid is led into a hydraulic output cylinder connected to the load through hydraulic lines. Thus, a unidirectional motion of the output cylinder shaft is obtained. In a practical situation, there is a need for bidirectional motion of the load and this can be implemented through the use of mechanical valves (Ellison, 2004) or MR fluid-based valves (Yoo et al., 2005). The hydraulic circuit has an accumulator on the low pressure side, which is used to apply bias pressure to the circuit and to filter out high frequency pressure oscillations. The stack is held between the preload base and the piston. Preload can be applied to the stack using a set screw arrangement inside the preload base. Since the length was nominally the same for each of the four active material stacks, the same pump body was used for all cases. The field generating coil for magnetostrictive stacks was designed to fit inside the pump body of the same pump. Thus, the overall dimensions of the actuator were the same for all four stacks. The salient features of this actuator are listed in Table 2. An isometric view of the pump showing its various components is shown in Figure 4.

The detailed operating procedure is as follows. The active material stack is mounted inside the pump body, as shown in Figure 4. In the case of the magnetostrictive stacks, the coil and the stack were designed to fit the same pump body. The hybrid actuator was then filled with the hydraulic fluid through a reservoir connected to the accumulator port and degassed thoroughly using a vacuum pump. Degassing is very critical to the performance of the pump since dissolved air decreases the bulk modulus of the fluid thus decreasing the amount of work that can be done on to the load. Compressibility in the transmission fluid decreases the overall efficiency of the system. The reservoir was then disconnected from the pump manifold and a bias pressure of 1.4 MPa (200 psi) was applied

Downloaded from http://jim.sagepub.com at UNIV OF MARYLAND on August 3, 2009

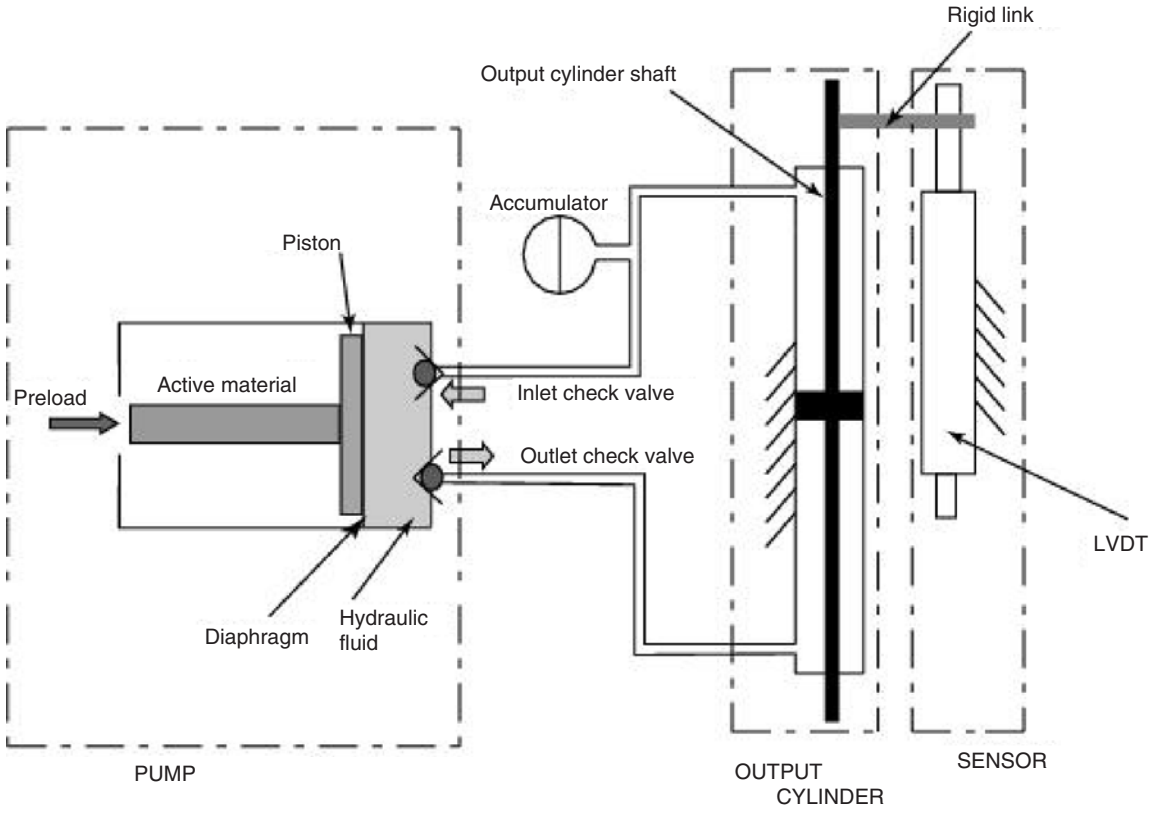

Figure 3. *Schematic diagram of the components of the hybrid hydraulic actuator.*

via an accumulator. The bias pressure mitigates the effects of entrained air and also applies a preload to the active material stack. Another major reason for application of bias pressure is to prevent cavitation in the hydraulic fluid. Cavitation will result in vaporization of the hydraulic fluid and the resulting two-phase system will cause a decrease in the performance of the actuator. The preload base was screwed tightly onto the pump body and the preload on the active material was further increased by tightening the set screw inside the preload base. The amount of applied preload was monitored using a strain gage mounted on the stack. This basic procedure was identical for both electro-active and magneto-active stacks.

In the case of electro-active materials, the stack was actuated using an amplified DC-biased sine signal of a particular frequency. The DC bias is required since electric fields with a polarity opposite to that of the poling direction of the stack can depole the material. In the case of magnetostrictive stacks, a pure sinusoidal signal of a particular frequency was sent to a power amplifier, which provided the coils with the necessary current to produce the magnetic field for actuation. There is no danger of depoling in the case of magnetostrictive materials. As mentioned earlier, due to the quadratic dependence of strain on the applied field, a pure sinusoidal input signal will produce a magnetic field at twice its frequency in the stack, and hence, induced strain also at twice the frequency. The resulting motion of the output cylinder shaft was measured using a TR50 Novotechnik linear potentiometer. The voltage amplifier used was AE Techron,

Table 2. Pump properties.

Pump body assembly	
Pump body diameter (mm, in.)	35.6, 1.4 O.D., 25.4, 1 I.D.
Pump body length (mm, in.)	50.8, 2
Piston diaphragm thickness (mm, in.)	0.05, 0.002
Pumping chamber diameter (mm, in.)	25.4, 1
Pumping chamber height (mm, in.)	0.76, 0.030
Valve assembly	
Valve plate thickness (mm, in.)	5.1, 0.2
Reed valve thickness (mm, in.)	0.051, 0.002
Hydraulic circuit	
Accumulator gas volume (mm^3, $in.^3$)	1638.7, 0.1
Output cylinder bore (mm, in.)	11.1, 7/16
Output shaft diameter (mm, in.)	1.58, 3/16
Output cylinder stroke (mm, in.)	50.8, 2
Coil parameters	
Wire gauge	20
Wire diameter (mm, in.)	0.02, 0.00081
Coil length (mm, in.)	50.8, 2
Coil diameter (mm, in.)	22.86, 0.9
Total mass (g)	113
DC resistance (Ω)	1.2
Inductance (mH)	2.1

Downloaded from http://jim.sagepub.com at UNIV OF MARYLAND on August 3, 2009

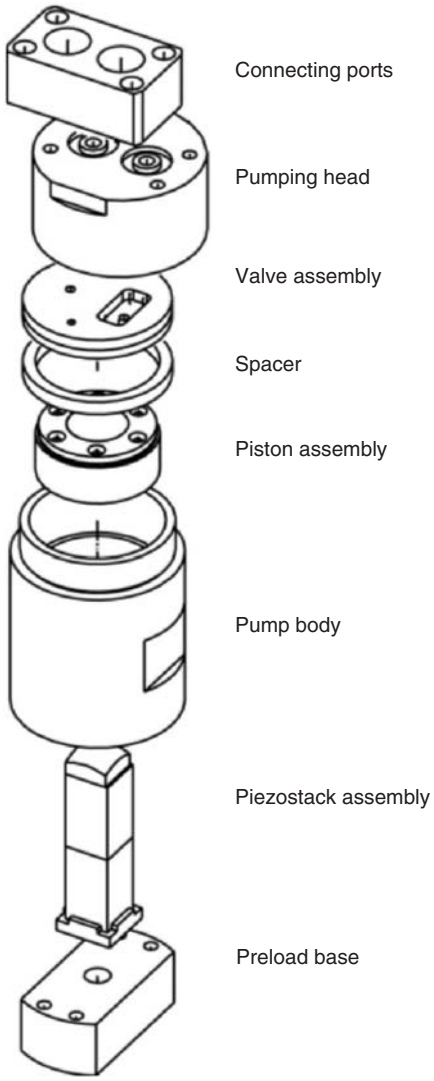

Figure 4. *Isometric view of the prototype hybrid actuator.*

LV 3620 Linear Amplifier. The current amplifier used was a commercially available audio amplifier QSC Audio RMX 2450 Professional Power Amplifier. All the data acquisition and appropriate signal generation was done through a dSPACE Autobox Real Time system.

Three types of tests were performed on each stack:

1. *Static tests:* The static tests were performed on the active material stack (but not on the actuator system). The objective of these tests was to determine the maximum free strain obtainable from the material under normal operating conditions and the calibration of the strain gage on the stacks. This test also served to verify the free strain values specified by the manufacturer. In the case of electro-active materials, a constant DC voltage was applied to the stack and the displacement was measured through the use of a laser sensor and corroborated with the signal received from a quarter-bridge strain gage that was mounted on the stack. The power amplifier used for the testing of magneto-active stacks was an audio amplifier. Since audio amplifiers are typically not capable of amplifying DC signals, only a quasi-steady test could be performed on the magneto-active stacks. Hence, a sinusoidal signal of very low frequency ($\ll$1 Hz) was amplified and applied across the field generating coil. This produced a very slowly varying magnetic field and simulated a quasi-steady condition. Elongation of the stack was then measured using a laser sensor and compared with the corresponding strain gage data.
2. *No-load tests:* These tests determine the flow rate generated by the active material in the absence of any external load. The flow rate was determined by measuring the shaft velocity of the output cylinder. Since the active material was not working against an external load, useful power output was zero. The input power was used to overcome the internal losses in the actuator and to accelerate the mass of the shaft and piston inside the output cylinder. Additionally, hysteresis curves obtained from no-load tests can be used to ascertain the amount of energy dissipation in the material.
3. *Loaded tests:* These tests were done to measure the performance of the pump in the presence of external loads. Graduated weights were hung from the shaft of the output cylinder to simulate the effect of external loads. Upon actuation of the active material, the output cylinder shaft moves, along with the load, at a particular velocity. By measuring the output velocity of the load, we can determine the useful power output from the actuator. This was done for various pumping frequencies and loads. The weights were gradually increased till the blocking load for the actuator was reached. This data was then used to deduce the load line and output power of the actuator. The input power to the actuator was also measured at each tested pumping frequency.

RESULTS

Static Tests

As mentioned in the previous section, static tests were performed on the different stacks to experimentally identify the maximum value of free strain obtainable from the sample within the safe operating range specified by the manufacturer. For electro-active stacks, this test was performed by applying a constant DC voltage to the stacks. This was done using a DC power supply capable of supplying voltages up to 400 V. Figure 1(a) shows the results for PZT and PMN stacks. We see that the PZT stack (rated for maximum 150 V) exhibited strain of 1300 μs at 140 V and the PMN stack

Downloaded from http://jim.sagepub.com at UNIV OF MARYLAND on August 3, 2009

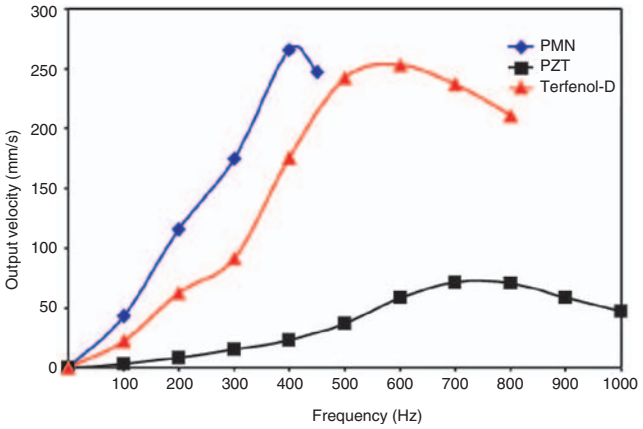

Figure 5. *Comparison of no-load output velocity for PMN, PZT, and Terfenol-D stacks as a function of pumping frequency.*

(rated for a maximum voltage of 500 V) gives a strain of 1600 μs at an excitation voltage of 350 V. To ensure the integrity of the stacks during further dynamic tests, the values of voltage used for static testing were less than the maximum rated operating voltages. From these values, we can say with sufficient confidence that the maximum free strain values provided by the manufacturer are accurate. Figure 1(b) shows the results of quasi-static tests performed on the magnetostrictive samples. The stack was placed inside the magnetic field generating coil such that the magnetic field lines run along the length of the stack. A very slowly varying magnetic field was applied to the stack (a very low frequency). The Terfenol-D stack shows a strain of 750 μs at a current of 4 A, while the Galfenol stack shows a strain of only 250 μs at a current of 0.5 A. We can see evidence for the slow varying nature of the magnetic field in the hysteresis loops in the quasi-steady data. The stacks were not tested beyond these values of current as the quasi-static curve showed signs of saturation at the higher values of current. Also, the ohmic heating produced in the coil at these high values of current is substantial. Sufficient time has to be provided between tests to sufficiently cool the field generating coil.

The free strain values provided by the manufacturer were verified via these static tests. Thus, we conclude the PMN stack exhibits the maximum free strain (of about 2000 με), followed by PZT (1600 με), Terfenol-D (1000 με), and Galfenol (300 με). We can see from these values that the free strain obtained from PMN was 25% greater than PZT and 100% greater than Terfenol-D stacks and that the strain obtained from Galfenol was 70% less than that of the Terfenol-D stack. Purely by consideration of volumetric displacement, we could conclude that PMN will produce the greatest velocity in the output cylinder shaft under no-load conditions. However, when the stack is pushing the fluid enclosed inside the pumping chamber, the force that the fluid exerts on the stack is also important. Thus, volumetric displacement alone does not determine the work output of the actuator. The free strain has to considered together with the stiffness of the stack to determine the amount of energy that is transferred by the stack to the hydraulic fluid and ultimately to the load.

No-load Tests

During no-load testing, the output cylinder shaft was permitted to move freely in the absence of any external load. No useful work was done during these tests and all the energy transferred by the stack to the fluid goes towards overcoming internal viscous losses in the pumping chamber and fluid paths in the actuator, frictional losses in the O-rings and lip seals in the output cylinder shaft, and in the motion of the shaft and piston mass of the output cylinder. In these tests, the active material was first mounted inside the pump body and preloaded. The stack was then actuated at various pumping frequencies causing the output cylinder shaft to move at different velocities. The velocity of the output cylinder shaft was measured using an LVDT. Figure 5 shows the comparison of velocity under no-load conditions for PZT, PMN, and Terfenol-D.

From this figure, we can see that the PMN stack produces the highest no-load velocity of 270 mm/s. The Terfenol-D stack also has a very high no-load velocity of 250 mm/s. The PZT stack has the least no-load velocity of about 70 mm/s. As mentioned earlier, the amount of energy transferred between the stack and the fluid is dictated by the free displacement and the stiffness of the stack in comparison with the stiffness of the fluid column in the pumping chamber. The stiffness of the fluid in the pumping chamber is given by Equation (1).

$$k_{\text{fluid}} = \frac{\beta A}{l} \tag{1}$$

where, k_{fluid} is the stiffness of the fluid column in the pumping chamber, β is the bulk modulus of the fluid, A is the area of cross-section of the pumping chamber, and l is the height of the pumping chamber. Using the geometrical values of the pump used in this study from Table 2 and a bulk modulus of 137.9 MPa (20000 psi), we obtain a fluid stiffness of 140 MN/m. When we compare this value of fluid stiffness to the values of stack stiffness listed in Table 1, we can see that all the stacks are considerably softer than the fluid column. Since none of the stacks have a more favorable impedance matching condition than the others, we can conclude that the highest no-load velocity shown by the PMN stack is due to its superior free strain capability compared to the other stacks. However, we see that the PZT stack shows a much lower no-load velocity than Terfenol-D, despite the fact that its free strain value is higher. The reason for this lies in the way in which stacks

Downloaded from http://jim.sagepub.com at UNIV OF MARYLAND on August 3, 2009

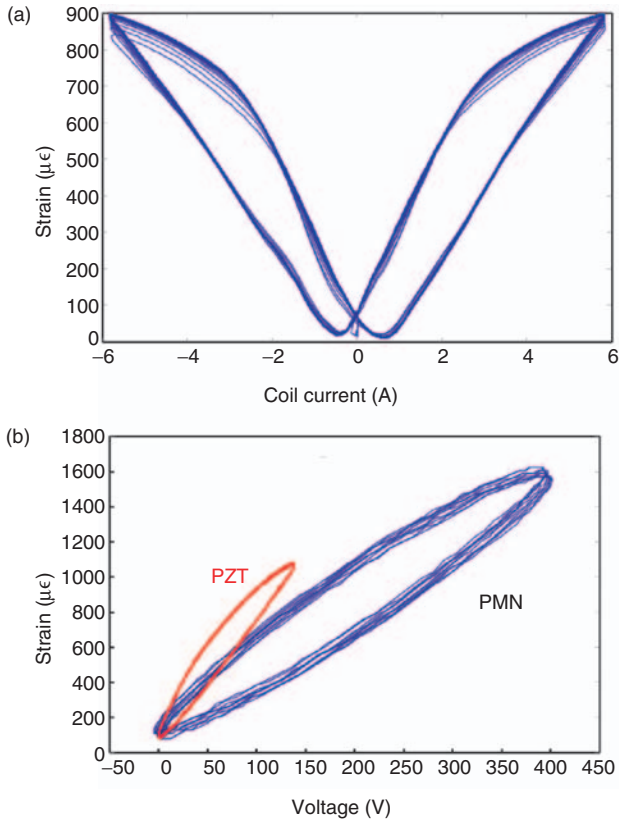

Figure 6. *Hysteresis loops obtained for Terfenol-D, PMN, and PZT stacks when driven at a pumping frequency of 100 Hz; (a) magneto-active stacks and (b) electro-active stacks.*

are made. Adjacent layers of piezoelectric material are glued together with alternating layers of insulating material to prevent short circuiting between the layers. The type and thickness of each insulating material layer depends on the choice of the manufacturer. Hence, the overall stiffness of the stack depends on the relative stiffness of the piezoelectric material and the insulating material. Since the value of overall stiffness of a stack is not provided by the manufacturer, the values listed in Table 1 were calculated considering a stack which consists only of the pure material. Magnetostrictive stacks are not affected by this issue as they are not made by layering the active material. Magnetostrictive material are usually single-crystalline or polycrystalline bulk material grown in cylindrical or cuboidal form. Though the Young's modulus of the raw PZT material is greater than that of PMN or Terfenol-D, the overall stack stiffness of PZT was lesser than PMN or Terfenol-D, thus lowering its no-load velocity. This factor will also manifest itself in load tests as a decrease in the output power.

These tests also enable us to compare the hysteresis characteristics of the different active materials. Hysteresis quantifies the internal material losses within the stack and is a characteristic of the material. The area under a hysteresis plot is indicative of the amount of energy lost internally in the material due to rearrangement of domains and polarized particles. Figure 6(a) shows the hysteresis curve of the Terfenol-D sample at 100 Hz. This plot shows the variation of strain with the current supplied to the coil. We can see that hysteresis curve of Terfenol-D has a characteristic butterfly shape showing a quadratic behavior, wherein a negative magnetic field produces a positive strain in the stack. Figure 6(b) shows the hysteresis characteristics of PMN and PZT stacks and plots the variation of strain with the applied voltage. We can quantify the hysteresis by normalizing the area under the hysteresis plot by the product of the peak values of voltage and strain. This quantity gives the area enclosed by the hysteresis loop as a fraction of the area of the smallest rectangle which encloses the loop. The value of this normalized hysteresis index is 0.18 for PMN and 0.06 for PZT. Thus, we can conclude that PMN exhibits higher hysteretic losses than PZT.

When the stacks were placed inside the pump and tested, the Galfenol stack failed to move the output cylinder shaft. Considering the low free strain shown by Galfenol, the lack of sufficient volumetric displacement of fluid to overcome the internal friction in the actuator could be a possible reason. This becomes evident from Figure 7. In this experiment, Terfenol-D was placed inside the pump and actuated by providing varying values of current to the coil. The output velocity was measured for progressively decreasing values of coil current. As the coil current decreases, the magnetic field applied to the stack decreases and induced strain decreases. This causes a decrease in the no-load output velocity. The applied magnetic field is decreased till the output cylinder shaft just tends to move. At this value of magnetic field, the stack produces just enough volumetric displacement in the hydraulic fluid to overcome the various internal frictions in the actuator. Consequently, magnetic fields below this value fail to produce any motion in the output cylinder shaft. Figure 7 shows that when the magnetic field applied to the Terfenol-D stack was decreased to give a strain of 400 μs, the actuator does not produce any output motion. Thus, we can conclude that the Galfenol stack, which gives a maximum free strain of 300 μs, does not produce sufficient volumetric displacement in the fluid chamber to produce output motion in the particular actuator design that was used in this study. As a result, Galfenol was not tested further in this study. However, Galfenol would be a promising and feasible material for an actuation system with lower internal friction. The nonlinear nature of the trend in Figure 7 is due to the Coulomb damping in the output cylinder shaft and piston. The effect of this frictional force becomes a more significant part of the total force as the forcing from the active element is reduced.

Downloaded from http://jim.sagepub.com at UNIV OF MARYLAND on August 3, 2009

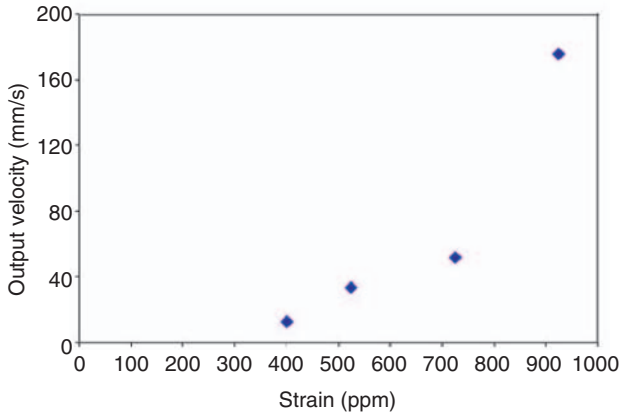

Figure 7. *The results of output velocity vs the strain generated in a Terfenol-D stack.*

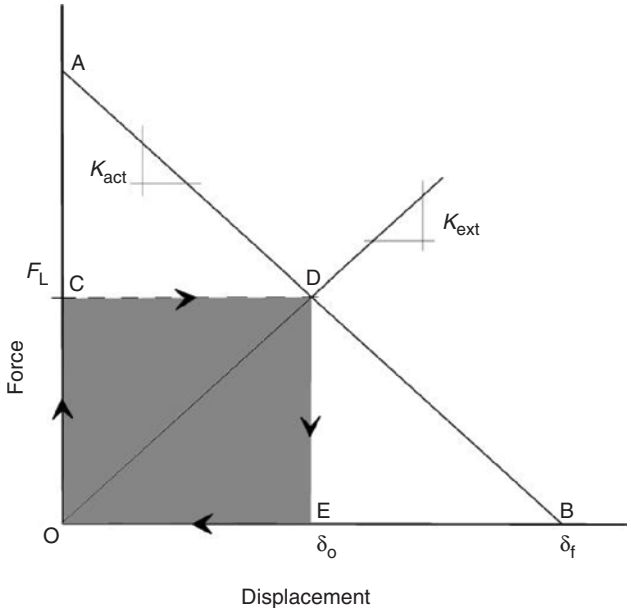

Figure 8. *Typical load line diagram of an actuator.*

Load Tests

Load tests were performed to ascertain the capability of different active materials to do useful work. In these tests, graduated weights are hung from the output cylinder shaft. When the active material was actuated, the output cylinder shaft lifted the weight, thus performing useful work. The output power of the actuator system can be calculated by multiplying the load by the shaft velocity. As the output load increases, the actuator reaches the block force limitations of the active material stack. The blocking load of the actuator system depends on the block force of the active material stack and the ratio of the cross-sectional areas of the output cylinder piston to that of the pumping chamber. The information gained from the relationship between output velocity and output load can be used to plot load lines at particular pumping frequencies.

Figure 8 shows a typical load line curve for an active material driven actuator. A load line is drawn at a particular pumping frequency and plots the variation of output velocity with the load. For pumping frequencies below the fluid resonance point, load lines are typically linear. This is due to the fact that the load line of the actuator bears a close relationship with the static load line of the active material, which is typically linear. Point A represents the blocked force of the actuator while point B denotes free displacement in the absence of load. The line OD denotes the stiffness of all the elements of the actuator, namely that of the hydraulic fluid, active material stack, accumulator and the piston diaphragm. The intersection point D marks the static equilibrium point for the whole system. As the voltage to the active material is varied, the load line shifts upwards, while remaining parallel to the original load line and the equilibrium point shifts along the line OD. In a loaded operation, energy is transferred from the active element to the load and is shown in Figure 8 as OCDEO, and the work done by the active material per cycle is the area shown in the shaded region. Thus, the maximum work obtainable from the actuator at a particular pumping frequency can be obtained by calculating half of the area under the load line OABO. This method can been used to compare the output power of the stacks. Experimentally obtained load lines for PMN, PZT and Terfenol-D stacks are shown in Figure 9(a)–(c). These plots were obtained by actuating the active material at a particular frequency and changing the load on the output cylinder shaft. The measured output velocity is then plotted against the load to obtain the load line at that particular pumping frequency. We can infer from these figures that the blocking force of the PMN is highest among the three active materials considered. The blocking load of the PMN-based actuator was 13 lbs, while the blocking load of the PZT-based actuator was the least among the three active materials at 7 lbs. The Terfenol-D-based actuator showed a blocking load of around 10 lbs.

As explained in the previous paragraph, the maximum output power of the actuation system can be obtained from load lines by calculating one half of the area under the load line. A comparison of output power gives us a comparison of capacity of different actuators to do useful work. These power output values are plotted against pumping frequency in Figure 10. We see from the figure that PMN and Terfenol-D stacks have a maximum output power of around 2.5 W. We see that the maximum output power occurs at different pumping frequencies. Maximum power output is obtained at the resonant frequency of the actuator system. The resonant frequency of the actuator system depends on the stiffness of the active material stack, the dynamics of the hydraulic fluid lines in the system and the load.

Downloaded from http://jim.sagepub.com at UNIV OF MARYLAND on August 3, 2009

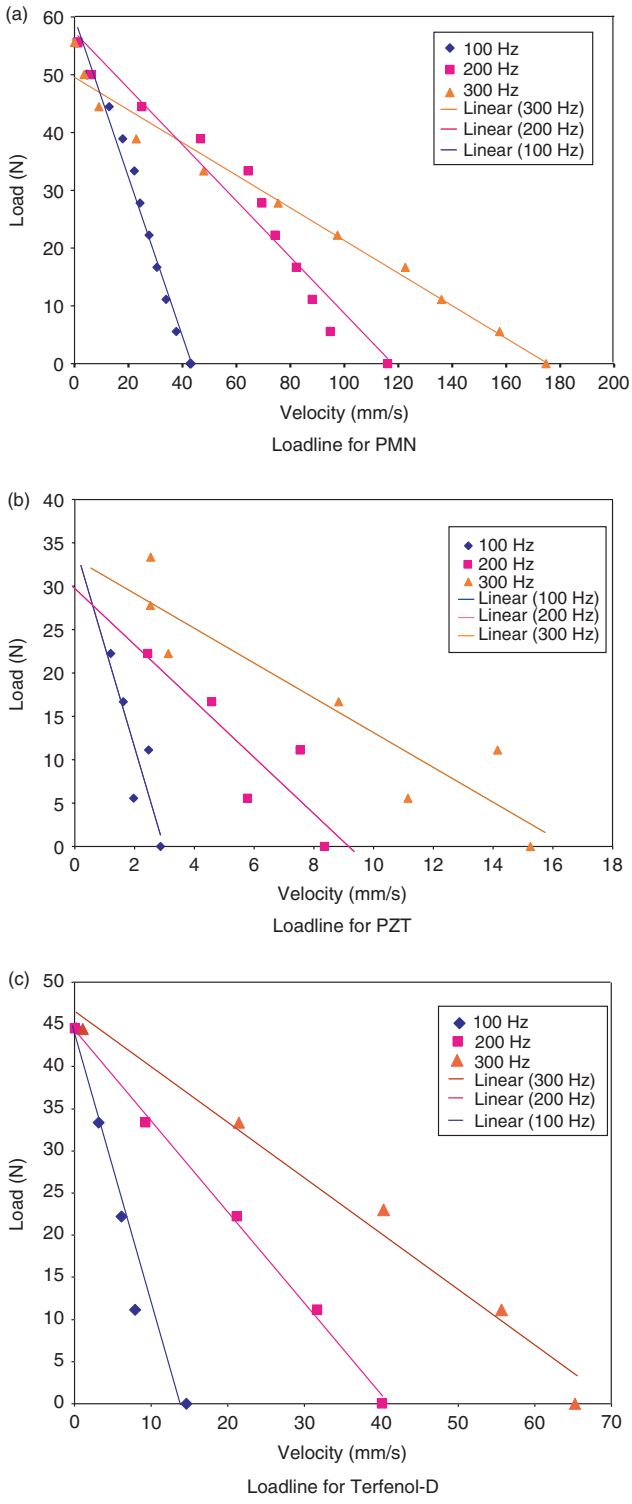

Figure 9. *Load lines for electro-active and magneto-active stacks as a function of pumping frequency (100, 200, and 300 Hz).*

Since the stiffness varied among different stacks tested in this study, the resonant frequencies are also different.

As the pumping frequency increased, the force exerted by the fluid on the stack also increased. This is due to higher inertial and damping forces of the fluid. The PMN and Terfenol-D stacks were able to sustain

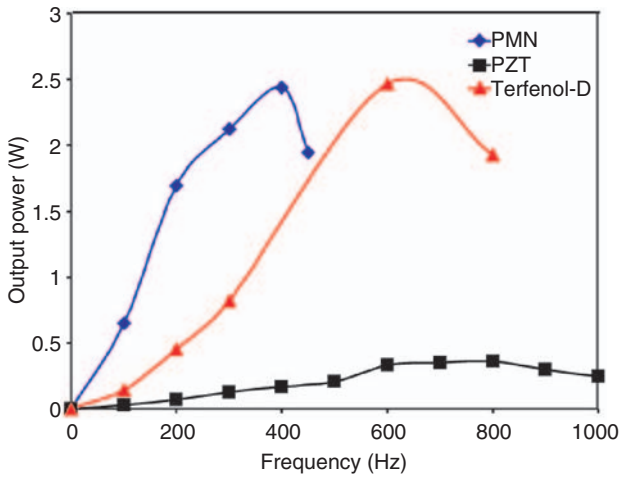

Figure 10. *Comparison of measured output power from the actuator driven by PMN, PZT, and Terfenol-D as a function of pumping frequency.*

substantial stack displacement even at higher pumping frequencies owing to their greater stack stiffness, thus exhibiting greater power output. Since the PZT stack is softer when compared with PMN and Terfenol-D stacks, it was not able to sustain the strain levels measured under quasi-steady conditions. The output power capability of the PZT stack was therefore lower than the other stacks at around 0.5 W at a pumping frequency of 700 Hz.

Overall Electromechanical Efficiency

Overall electromechanical efficiency defines the ratio of the amount of useful mechanical energy obtained from the actuation system to the electrical energy put into the active material stack. The input work is measured in terms of apparent power, which is defined as the product of the RMS values of voltage and current drawn by the active material stack. The power drawn by electro-active materials depends on the stack capacitance. Thus, the PZT stack requires greater input power than PMN for a given voltage, owing to its higher capacitance. The electrical power consumed by the magnetostrictive stacks is determined by the electric impedance of the coils. This electrical impedance appears as a predominantly inductive component from the coils and a resistance of the metallic wire used in the coil. Due to the large inductive component of the impedance, larger voltages are required to produce the same magnetic field over the active material at higher frequencies (since magnetic field produced by the coil is proportional to the current in the coil). This results in power losses as a result of eddy currents in the coils. The resistance of the coils also changes with temperature, thus altering the electrical impedance. Another major cause of power losses in magnetic

Downloaded from http://jim.sagepub.com at UNIV OF MARYLAND on August 3, 2009

circuits, in addition to ohmic losses, is eddy currents. As a result of alternating magnetic induction and a conducting magnetic flux return path, eddy current loops are generated. The formation of such loops cause power losses due to ohmic heating in the flux return paths. In the actuator used in this study, the pumping body, made of steel, was used as the magnetic flux return path and hence, forms an ideal conducting path for eddy currents. To prevent the effect of such current loops, a narrow slit was machined lengthwise in the pump body. This prevents the formation of such loops to a large extent and mitigates losses due to ohmic heating.

The current and voltage across the active material is recorded during load tests. This enables us to calculate the input power to the material. These experimental results obtained are shown in Figure 11. The PMN stack was tested only up to a maximum pumping frequency of 500 Hz to maintain the integrity of the stack (as recommended by TRS Ceramics Inc.). We see that at 200 Hz pumping frequency, the PMN-based actuator is five times as efficient as the PZT-based actuator and seven times more efficient than the Terfenol-D-based actuator. Though the PMN stack exhibits greater hysteretic losses than PZT, it is much more electromechanically efficient due to its lower power consumption.

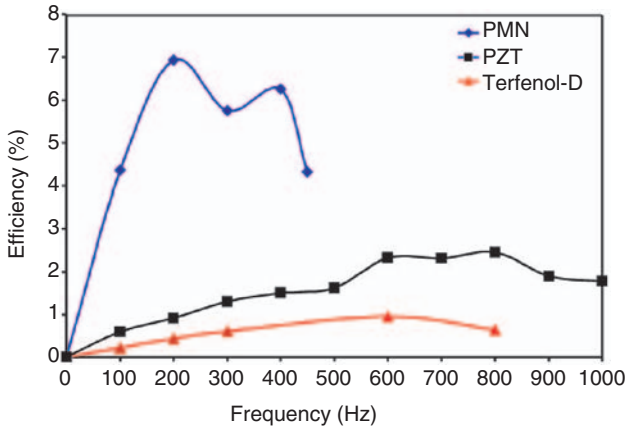

Figure 11. *Comparison of electromechanical efficiency of the hybrid actuator with PMN, PZT, and Terfenol-D as a function of pumping frequency.*

CONCLUSION

The goal of this study was to compare the actuator properties of two kinds of active materials – electro-active (PMN and PZT) and magneto-active (Terfenol-D and Galfenol) materials for our hydraulic hybrid actuator configuration. The materials were tested as active elements in a hybrid hydraulic actuator developed at the University of Maryland and their performance was evaluated in terms of metrics like static displacement, no-load velocity, output power, and electro-mechanical efficiency. Since most of the applications of such hydraulic hybrid actuators involve overall geometrical constraints, the overall length of the active material as well as the whole actuator system was held constant in all four cases.

The maximum static displacement obtained from the PMN stacks was around 100 μm (350 V). The free displacement of PMN was much higher than was obtained from PZT, Terfenol-D or Galfenol stacks. Greater free displacement results in greater volumetric displacement of fluid in the pump and this manifests as a higher no-load velocity. The maximum no-load velocity obtained with PMN stacks was 270 mm/s (at 400 Hz pumping frequency), while the PZT and Terfenol stacks generated a maximum no-load velocity of 75 mm/s (at 600 Hz pumping frequency) and 250 mm/s (at 600 Hz pumping frequency). The Galfenol stack failed to provide any output motion in the actuator system used for this study. This was due to the fact that the free strain capability of Galfenol was insufficient to overcome the internal frictional and stiffness losses in the actuator system.

The measured blocked force for the PMN actuator was around 13 lbs (57.8 N), the PZT actuator was 7.5 lbs (62.3 N) and Terfenol-D actuator was 10 lbs. The stiffness of the stack greatly influenced the blocked force of the actuator. Though the stiffness value of the PZT stack that was provided by the manufacturer is higher than PMN, the presence of insulating layers in the stack decreased its overall stiffness, thus making the blocked force much lower than that of a PMN-based actuator. From tests under load, output power and overall system efficiency was determined. The maximum power output from the PMN actuator was around 2.5 W at 400 Hz, the PZT actuator generated almost 0.5 W at 700 Hz pumping frequency and Terfenol-D generated 2.5 W at 600 Hz pumping frequency. However, the PMN actuator generated this power at a far greater efficiency than the PZT or Terfenol-D-based actuator. The overall electromechanical efficiency of the PMN actuator was around 7% at 200 Hz pumping frequency while the PZT and Terfenol-D-based actuators were only 2.5% and 0.5% efficient. Although the output power from the different materials was not very different, the low input power required for the PMN-based actuator improved its efficiency. Thus, PMN shows superior performance in terms of output power and overall electromechanical efficiency. A comparison of the major performance results are listed in Table 3.

Downloaded from http://jim.sagepub.com at UNIV OF MARYLAND on August 3, 2009

Table 3. Performance results.

Parameter	PZT	PMN	Terfenol-D	Galfenol
Blocked force (N, lbs)	33.7, 7.5	57.8, 13	44.5, 10	–
Maximum no-load velocity (mm/s)	75	270	250	–
Maximum output power (W)	0.5	2.5	2.5	–
Maximum efficiency (%)	2.5	7	0.5	–
Mass of active material (g)	13.6	16.8	14.8	11.2
Mass of coil (g)	NA	NA	113	113

ACKNOWLEDGMENTS

This research was supported by the U.S. Army Research Office under a Phase 2 STTR contract W911NF04C0115 (Dr Gary Anderson, Technical Monitor) and by the U.S. Army Aviation Applied Technology Directorate under a Phase 1 SBIR Contract W911W6-05-C-0037 (Dr Louis Centolanza, Technical Monitor). Additional support was provided by DARPA under sponsor No. F3361503C3320 (Dr John Main, DARPA, Technical Monitor). The authors would like to thank Dr Thomas Lograsso of Ames Laboratory (Ames, Iowa) for providing the Galfenol stacks.

REFERENCES

Cadou, C. and Zhang, B. 2003. "Performance Modeling of a Piezo-Hydraulic Actuator," *Journal of Intelligent Material Systems and Structures*, 14(3):149–160.

Damjanovic, D. and Newnham, R.E. 1992. "Electrostrictive and Piezoelectric Materials for Actuator Applications," *Journal of Intelligent Material Systems and Structures*, 3(2):190–208.

Duong, J. and Garcia, E. 1996. "Design and Performance of a Rotary Motor Driven by Piezoelectric Stack Actuators," *Japanese Journal of Applied Physics, Part 1*, 35(12A):6334–6341.

Ellison, J. 2004. Investigation of Active Materials as Driving Elements in a Hydraulic-hybrid Actuator, Master's Thesis, University of Maryland, College Park, MD, USA.

Frank, J.E., Mockensturm, E.M., Koopmann, G.H., Lesieutre, G.A., Chen, W. and Loverich, J.Y. 2003. "Modeling and Design Optimization of a Bimorph-driven Rotary Motor," *Journal of Intelligent Material Systems and Structures*, 14(4–5):217–227.

Galante, T., Frank, J.E., Bernard, J., Chen, W., Lesieutre, G.A. and Koopmann, G.H. 2000. "Design, Modeling, and Performance of a High Force Piezoelectric Inchworm Motor," *Journal of Intelligent Material Systems and Structures*, 10(12):962–972.

Hemsel, T. and Wallaschek, J. 2000. "Survey of the Present State of the Art of Piezoelectric Linear Motors," *Ultrasonics*, 38(1–8):37–40.

Janocha, H., Schaefer, J.J.D. and Jendritza, J. 1994. "Piezoelectric and Magnetostrictive Materials for use in Smart Actuators," In: *Proceedings of the Joint Hungarian – British International Mechatronics Conference*, September 21–23, Budapest, Hungary, pp. 397–404.

John, S., Cadou, C., Yoo, J.-H. and Wereley, N. 2006. "Application of CFD in the Design and Analysis of a Piezoelectric Hydraulic Pump," *Journal of Intelligent Material Systems and Structures*, 17(11):967–979.

Konishi, K., Ukida, H. and Kotani, T. 1997. "Hydraulic Actuators Driven by Piezoelectric Elements (4th report, Construction of Mathematical Models for Simulation)," *Journal of Japanese Society of Mechanical Engineering (C)*, 63(605):158–165.

Konishi, K., Ukida, H. and Sawada, K. 1998. "Hydraulic Actuators Driven by Multilayered Piezoelectric Elements – Mathematical Model and Application to Brake Device," In: *Proceedings of the 13th Korean Automatic Control Conference*, pp. 474–479.

Lam, A.H.-F. and Liao, W.-H. 2003. "Semi-Active Control of Automotive Suspension Systems with Magneto-rheological Dampers," *International Journal of Vehicle Design*, 33(1–3):50–75.

Mauck, L., Oates, W. and Lynch, C. 2001. "Piezoelectric Hydraulic Pump Performance," In: *Proceedings of the SPIE – Smart Structures and Materials 2001 – Industrial and Commercial Applications of Smart Structures Technologies*, Vol. 4332, pp. 246–253.

Mauck, L.D. and Lynch, C.S. 2000. "Piezoelectric Hydraulic Pump Development," *Journal of Intelligent Material Systems and Structures*, 11(10):758–764.

Nasser, K. and Leo, D. 2000. "Effciency of Frequency-rectified Piezohydraulic and Piezopneumatic Actuation," *Journal of Intelligent Material Systems and Structures*, 11(10):798–810.

Nasser, K., Leo, D.J. and Cudney, H.H. 2000. "Compact Piezohydraulic Actuation System," In: *Proceedings of the 7th SPIE Conference on Smart Structures and Integrated Systems*, Vol. 3991, pp. 312–322.

Oates, W. and Lynch, C. 2001. "Piezoelectric Hydraulic Pump System Dynamic Model," *Journal of Intelligent Material Systems and Structures*, 11:798–810.

Pan, M.-J., Rehrig, P.W., Kucera, J.P., Park, S.-E. and Hackenberger, W.S. 2000. "Comparison of Actuator Properties for Piezoelectric and Electrostrictive Materials," In: *Proceedings of SPIE – The International Society for Optical Engineering, Smart Structures and Materials 2000 – Active Materials: Behavior and Mechanics*, Vol. 3992, pp. 80–90.

Pomirleanu, R. and Giurgiutiu, V. 2004. "High-Field Characterization of Piezoelectric and Magnetostrictive Actuators," *Journal of Intelligent Material Systems and Structures*, 15(3):161–180.

Prechtl, E. and Hall, S. 1999. "Design of a High Efficiency, Large Stroke, Electromechanical Actuator," *Smart Materials and Structures*, 8(1):13–30.

Regelbrugge, M., Lindler, J. and Anderson, E. 2003. "Design Model for Piezo-hydraulic Actuators," In: *Proceedings of the 44th AIAA/ASME/ASCE/AHS/ASC Structures, Structural Dynamics and Materials Conference*, Vol. 3, pp. 2163–2171.

Sashida, T. and Kenjo, T. 1993. *An Introduction to Ultrasonic Motors*, Claredon Press, Oxford.

Shoji, S. and Esashi, M. 1994. "Microflow Devices and Systems," *Journal of Micromechanics and Microengineering*, 4(4):157–171.

Sirohi, J. 2002. Piezoelectric Hydraulic Hybrid Actuator for a Potential Smart Rotor Application, PhD Thesis, University of Maryland, College Park, MD, USA.

Downloaded from http://jim.sagepub.com at UNIV OF MARYLAND on August 3, 2009

Sirohi, J., Cadou, C. and Chopra, I. 2005. "Investigation of the Dynamic Characteristics of a Piezohydraulic Actuator," *Journal of Intelligent Material Systems and Structures*, 16(6):481–492.

Sirohi, J. and Chopra, I. 2003. "Design and Development of a High Pumping Frequency Piezoelectric–Hydraulic Hybrid Actuator," *Journal of Intelligent Material Systems and Structures*, 14(3):135–147.

Uchino, K. 1997. *Piezoelectric Actuators and Ultrasonic Motors*, Kluwer Academic Publishers, Boston.

Yoo, J.-H., Sirohi, J. and Wereley, N.M. 2005. "A Magnetorheological Piezohydraulic Actuator," *Journal of Intelligent Material Systems and Structures*, 16(11–12):945–953.

Zhao, J. and Zhang, Q.M. 1996. "Effect of Mechanical Stress on the Electromechanical Performance of PZT and PMN-PT Ceramics," In: *Proceedings of the 1996 10th IEEE International Symposium on Applications of Ferroelectrics, ISAF'96. Part 2 (of 2)*, 18–21 August, East Brunswick, NJ, USA, Vol. 2, pp. 971–974.

Downloaded from http://jim.sagepub.com at UNIV OF MARYLAND on August 3, 2009